Prediction of Glioma Grade using Intratumoral and Peritumoral Radiomic Features from Multiparametric MRI Images

Jianhong Cheng, *Student Member, IEEE,* Jin Liu*, *Member, IEEE,* Hailin Yue, Harrison Bai,Yi Pan, *Senior Member, IEEE,* and Jianxin Wang*, *Senior Senior, IEEE*

Abstract—The accurate prediction of glioma grade before surgery is essential for treatment planning and prognosis. Since the gold standard (i.e., biopsy) for grading gliomas is both highly invasive and expensive, and there is a need for a noninvasive and accurate method. In this study, we proposed a novel radiomics-based pipeline by incorporating the intratumoral and peritumoral features extracted from preoperative mpMRI scans to accurately and noninvasively predict glioma grade. To address the unclear peritumoral boundary, we designed an algorithm to capture the peritumoral region with a specified radius. The mpMRI scans of 285 patients derived from a multi-institutional study were adopted. A total of 2153 radiomic features were calculated separately from intratumoral volumes (ITVs) and peritumoral volumes (PTVs) on mpMRI scans, and then refined using LASSO and mRMR feature ranking methods. The top-ranking radiomic features were entered into the classifiers to build radiomic signatures for predicting glioma grade. The prediction performance was evaluated with five-fold cross-validation on a patient-level split. The radiomic signatures utilizing the features of ITV and PTV both show a high accuracy in predicting glioma grade, with AUCs reaching 0.968. By incorporating the features of ITV and PTV, the AUC of IPTV radiomic signature can be increased to 0.975, which outperforms the state-of-the-art methods. Additionally, our proposed method was further demonstrated to have strong generalization performance in an external validation dataset with 65 patients. The source code of our implementation is made publicly available at https://github.com/chengjianhong/glioma_grading.git.

Index Terms—Glioma grade, radiomics, intratumoral volumes, peritumoral volumes.

1 Introduction

GLIOMAS are the most prevalent primary brain tumors of the central nervous system, accounting for 80% of malignant brain tumors in adults [1]. In clinical practice, treatment decisions usually need to be tailored to the grade of the tumor diagnosed. Generally, tumors are assigned World Health Organization (WHO) grades I-IV according to the aggressiveness of cancerous cells [2]. The WHO further classifies gliomas into two grades, i.e., low-grade gliomas (LGGs, grade I and II) and high-grade gliomas (HGGs, grade III and IV) [1], [2]. Accurate glioma grading is critical for making treatment options, implementing personalized therapy, and predicting prognosis and survival time [3], [4], [5], [6]. At present, the diagnosis of glioma grade is determined by surgical biopsy or histopathological analysis [1], [2]. However, this diagnostic method is invasive and limited for patients who are not suitable for surgery. Therefore, it is necessary to design a noninvasive and highly accurate glioma grading system.

Magnetic resonance imaging (MRI) has become a popular noninvasive means for radiologists to diagnose brain tumors over the past few years [7], [8], [9]. Although experienced radiologists can easily detect tumors from MRI sequences by the naked eye, it is difficult to identify glioma grade due to tumor heterogeneity. Recently, promising advances have been made using preoperative multiparametric magnetic resonance imaging (mpMRI) scans and the radiomics features extracted from these scans for grading gliomas. For example, Zacharaki et al. developed a computer-aided diagnosis (CAD) system to differentiate brain types using support vector machine-recursive feature elimination (SVM-RFE) [10]. Vamvakas et al. also utilized the SVM-RFE algorithm to select 21 radiomics features from mpMRI data for predicting glioma grade and achieved good performance with leave-one-out cross-validation on a small number of patient samples [11]. Reza et al. [12] employed radiomics-based methods and achieved a high sensitivity of 0.980 but a low specificity of 0.620 on a public dataset. Based on the same dataset, Cho et al. [13] found that two shape-based features (i.e., spherical disproportion and compactness) in intratumoral regions were essential for grading gliomas and achieved good performance with an AUC of 0.921. Despite the fact that the previous studies have made relatively great achievements in distinguishing HGG from LGG, extracting more valuable radiomic features to improve the prediction accuracy remains a challenge. Recently, a multicenter study showed that a high postoperative residual nonenhancing tumor volume conveyed a worse prognosis [14]. With the growing understanding of the prognostic importance of nonenhancing tumors in

J. Liu, H. Yue, and J. Wang are with the Hunan Provincial Key Lab on Bioinformatics, School of Computer Science and Engineering, Central South University, Changsha 410083, China, e-mail: {liujin06, yuehailin, and jxwang}@mail.csu.edu.cn.

J. Cheng is with the Hunan Provincial Key Lab on Bioinformatics, School of Computer Science and Engineering, Central South University, Changsha 410083, China, and the Institute of Guizhou Aerospace Measuring and Testing Technology, Guiyang 550009, China. e-mail: jianhong_cheng@csu.edu.cn.

H. Bai is with the Department of Diagnostic Imaging, Rhode Island Hospital and Alpert Medical School of Brown University, Providence, RI 02912 USA. e-mail: harrison_bai@brown.edu.

Y. Pan is with the Department of Computer Science, Georgia State University, Atlanta, GA 30302, USA. e-mail: yipan@gsu.edu.

glioblastoma (GBM), some experts have suggested expanding the scope of surgical resection to the nonenhancing tumors, not only enhancing tumors [15], [16]. These studies indirectly provide the possibility of improving accuracy by using nonenhancing tumors for grading gliomas.

However, the existing radiomics-based methods mainly focus on the intratumoral tumors and ignore the role of the peritumoral environment in the study of glioma grading [10], [13]. Significant clinical evidence [17] suggests that the heterogeneity of GBM is not limited to the tumor margins but also involves the peritumoral region, where approximately 90% of patients with GBM experience recurrence [18]. Another clinical study revealed that the interaction between specific cells (such as glioma cells, neuroglia, or vascular endothelial cells) and molecular events in the peritumoral region may contribute to hypoxia, angiogenesis, and tumor infiltration, ultimately leading to poor survival in GBM [19]. Therefore, the peritumoral environment of tumors is also promising and may provide valuable information for the clinical evaluation of the invasive biological behaviors of tumors [18], [20]. Recently, there have been some promising studies combining the peritumoral and intratumoral radiomic features to identify the intrinsic molecular subtypes of HER2+ breast cancers [21], predict response to chemotherapy [22] and lymph node metastasis [23] in lung adenocarcinoma, and distinguish adenocarcinomas from granulomas [24]. Researchers also found that peritumoral edema was closely related to the prognosis of glioma patients [25], [26]. Therefore, extracting and fusing the peritumoral and intratumoral features is a promising approach that provides an idea for glioma grading and may further improve the diagnosis or prediction performance of glioma grading.

Numerous deep learning-based studies have exhibited the potential for grading gliomas on medical images. Xiao et al. [27] used the features extracted from a pretrained deep learning model based on ImageNet in conjunction with conventional radiomic features to build a radiomic signature, the performance of which transcends that of the model solely based on radiomic or deep learning features. Similarly, the concept of deep transfer learning was adopted, and Deepak et al. and Yang et al. fine-tuned a pretrained GoogLeNet to extract features from brain MRI images for differentiating tumor types [28] and tumor grades [29], respectively. Yang et al. [29] achieved good performance with an AUC of 0.968 for grading gliomas in 131 private patients, outperforming the performance of GoogLeNet trained from scratch. Additionally, Milan et al. [30] designed a CAD system consisting of a fully automatic segmentation network to extract the glioma followed by grading using a 3D convolutional neural network. The encouraging performance of these deep learning-based methods is attributed to a large number of training samples, but it is widely regarded as a black-box lacking satisfactory interpretability [31], [32], [33], [34].

Based on the ideas mentioned above, we apply the promising radiomics-based approach combined with different machine learning methods to noninvasively characterize the glioma grade by using intratumoral and peritumoral radiomic features extracted from preoperative mpMRI scans. Our main contributions are summarized as following:

1) We designed an algorithm to capture the peritumoral region with a specified radius. This algorithm is implemented and seamlessly embedded into the PyRadiomics toolbox [35] for extracting peritumoral features.
2) We proposed a novel radiomics-based pipeline by incorporating the intratumoral and peritumoral features extracted from preoperative mpMRI scans to accurately and noninvasively predict glioma grade.
3) We evaluated our proposed method on the Multimodal Brain Tumor Segmentation Challenge (BraTS) 2017 dataset and investigated the predictive performance of radiomic signature based on intratumoral features, peritumoral features and their combinations.
4) We further validated our proposed method on an external validation dataset and presented the radiomic features with high predictive performance, which may provide new imaging biomarkers for grading gliomas.

The remainder of this paper is organized as follows. Materials and methods are introduced in Section 2. Experiments and results are presented in Section 3. A discussion of our works is provided in Section 4. Finally, a brief conclusion to this study is provided in Section 5.

2 Materials and Methods

In this section, we first introduce the data used in this study as well as the preprocessing methods. Then, we define intratumoral and peritumoral VOIs and introduce their segmentation algorithms. Moreover, the extraction of radiomic features, feature selection and classifier modeling are described in detail. Finally, the metrics used for evaluating are provided. The overall workflow of this study is shown in Fig. 1.

2.1 Data and preprocessing

The current study data was derived from the BraTS challenge. We used the data from BraTS 2017 training dataset to investigate glioma grading. The BraTS 2017 training dataset [36], [37], [38] comprises 285 preoperative mpMRI scans of patients with gliomas (210 HGGs and 75 LGGs) and is primarily derived from two subsets of The Cancer Genome Atlas (TCGA), i.e., the TCGA-GBM collection [39] and TCGA-LGG collection [40]. Additionally, we reorganized 65 preoperative mpMRI scans of patients with gliomas (48 HGGs and 17 LGGs) from a portion of BraTS 2019 dataset [36], [37], [38] as an external validation dataset. Of these datas, 48 HGGs and 1 LGG are derived from the BraTS 2019 training dataset, and the remaining 16 LGGs are derived from the BraTS 2019 validation dataset. We

TABLE 1: Summary of the dataset used in this study.

No. of patients	BraTS 2017	External validation
HGG	210 (73.68%)	48 (73.85%)
LGG	75 (26.32%)	17 (26.15%)
Total	285	65

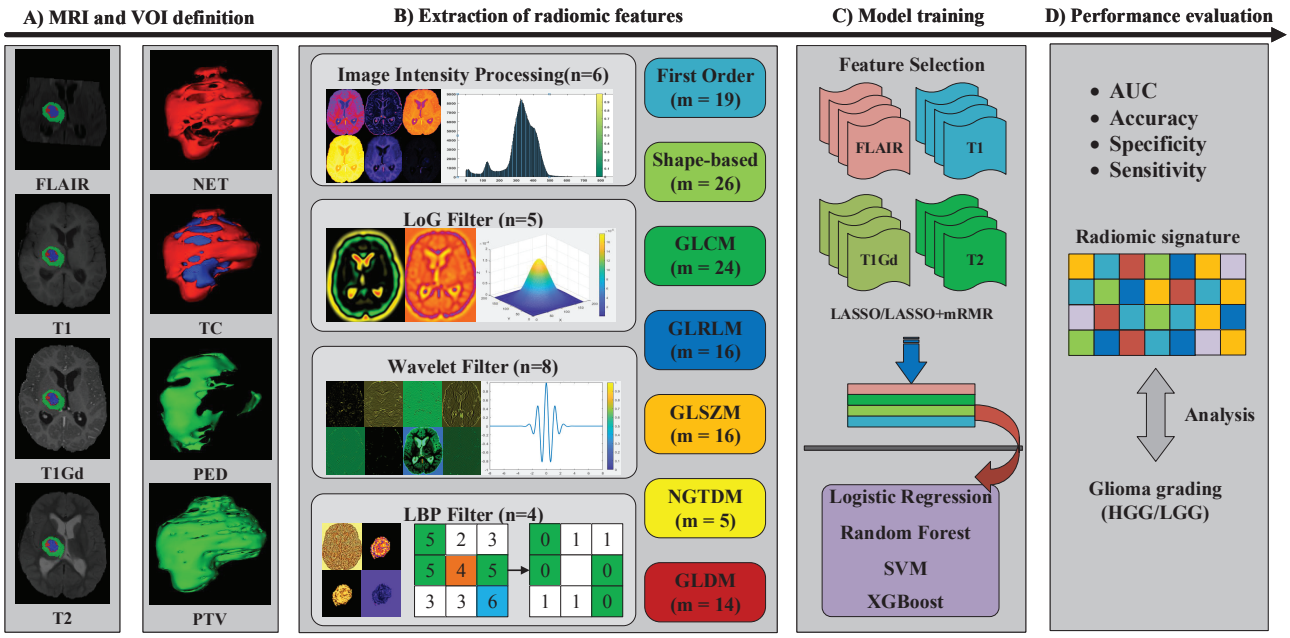

Fig. 1: Overall workflow of the entire study. **A) MRI and VOI definition**. mpMRI scans including FLAIR, T1, T1Gd, and T2 were used in this study. Two intratumoral volumes of interest on each MRI are defined as nonenhancing tumor (NET) and tumor core (TC), and the peritumoral volumes of interest on each MRI are defined as peritumor volumes (PTV, 5 mm around tumor core) and peritumoral edema(PED). **B) Extraction of radiomic features**. A total of 2153 radiomic features are calculated from each VOI on the mpMRI scans. **C) Model training**. The top-ranking radiomic features are determined by the LASSO and mRMR feature ranking methods and are entered into the classifiers to build radiomic signatures for glioma grading. **D) Performance evaluation**. The performance of radiomic signatures is measured by AUC, accuracy, specificity, and sensitivity.

confirm that there is no overlap between the BraTS 2017 training dataset and the external validation dataset. All of them are publicly available in The Cancer Imaging Archive (TCIA) and BraTS challenge. The summary of the dataset used in this study is summarized in Table 1. Each subject has four modalities: T1-weighted (T1), postcontrast T1-weighted (T1Gd), T2-weighted (T2) and T2 fluid-attenuated inversion recovery (FLAIR) volumes. To overcome the influence among patients, all preoperative mpMRI scans were first reoriented to the LPS (left-posterior-superior) coordinate system, coregistered to the same T1 anatomical template, resampled into a uniform isotropic voxel size of 1 $mm \times 1$ $mm \times 1$ mm, and skull-stripped using the brain extraction tool [37].

2.2 VOI definition and segmentation

According to the clinical studies, the BraTS organizers have delineated three volumes of interest (VOIs), i.e., the enhancing part of the tumor core (ET), the necrotic (fluid-filled) and nonenhancing part of the tumor core (NET), and the peritumoral edema (PED) [37]. In terms of appearance, ET shows hyperintensity in T1Gd compared with T1 scans. In contrast, the appearance of necrosis (NCR) and NET presents hypointense in T1Gd compared to T1 scans. Additionally, PED is described by hyperintense signal in the FLAIR scan. In the BraTS 2017 dataset, manual annotations of these VOIs were performed using a computer-aided segmentation approach with domain experts [39], [40]. In the external validation dataset, the VOIs of 48 HGGs and 1 LGG were annotated using the above method, and those of the remaining 16 LGGs were firstly extracted using DMFNet which performed well in the glioma segmentation task [41]. Then, these VOIs were further manually corrected and annotated by a radiologist with eight years of experience. Finally, the labels given in each scan are 1 for NCR and NET,

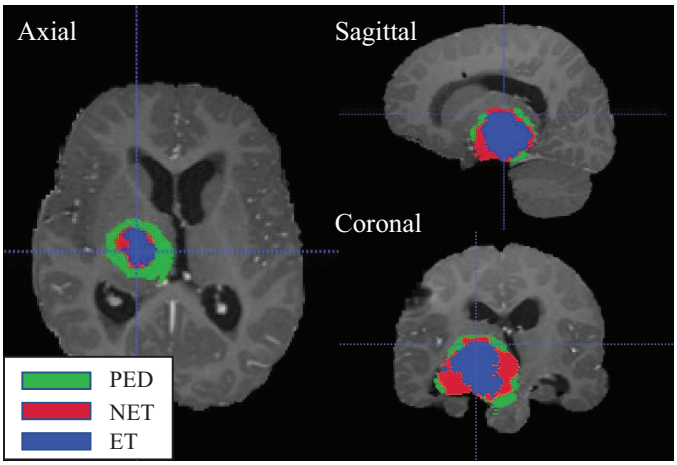

Fig. 2: A segmentation diagram on an axial, sagittal and coronal view of the T1Gd volume. PED denotes the peritumoral edema, NET denotes a nonenhancing tumor and ET denotes an enhancing tumor. The combination of NET and ET forms TC.

Algorithm 1 Calculating the image and mask of the peritumoral volume.

Input: The original 3D medical image I, and the corresponding tumor core mask M_{tc}; the region outside of the tumor core with radial distances of r mm.

Output: The image and mask of the peritumoral volume with a size of r, P_r, M_P.

1: Defining a structural element B with a specified size and shape; the size is equal to $2r + 1$, and the shape can be chosen for different types, such as the rectangular, cross, and ellipse.
2: Compute the number of slices of the original image mask in the axial direction n.
3: **for** $i \leftarrow 1$ to n **do**
4: $M_d[:, :, i] \leftarrow M_{tc}[:, ; , i] \bigoplus B$ // morphological operation of dilation;
5: **end for**
6: The mask of peritumoral volume: $M_p \leftarrow M_d - M_{tc}$;
7: $P_r = I \bigodot M_P$ // matrix dot product operation;
8: **return** P_r, M_P.

2 for PED, 4 for ET, and 0 for everything else [37], [38]. However, according to statistics, some patients,especially LGG patients, do not have enhancing tumors on MRI images. Fig. 2 shows a segmentation diagram of the T1Gd volume. To comprehensively investigate the effect of intratumoral volumes (ITVs) on grading gliomas, we define the following two VOIs based on existing annotations.

1) The tumor core (TC) region includes all intratumoral structures except edema (i.e., label 1 and label 4).
2) The nonenhancing tumor (NET) region only contains the nonenhancing tumor structure (i.e., label 1).

Additionally, we hypothesize that the radiomic features from the peritumoral region are associated with glioma grade. Beacuse the peritumoral boundaries are unclear and difficult to differentiate with morphologic imaging, obtaining the mask and size of the peritumoral volumes (PTVs) is a challenge. To address this problem and investigate the effect

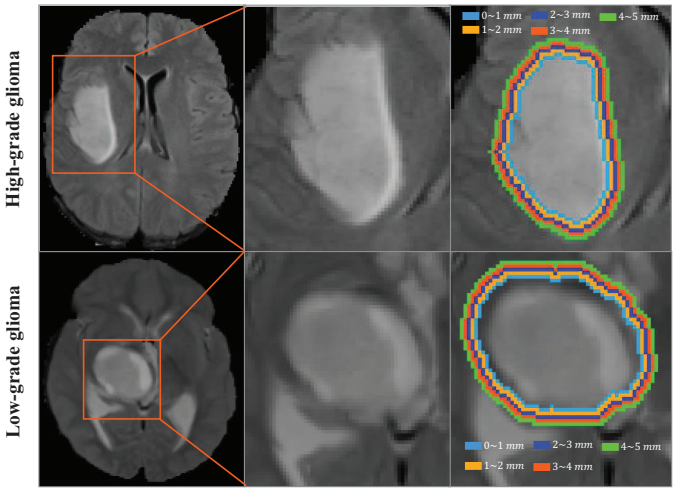

Fig. 3: Peritumoral region segmentation with various intervals (up to 5mm) from which radiomic features are extracted. This region is an annular ring.

of PTV on grading gliomas, we developed a method to capture the volumes outside the tumor core at intervals of 1 mm up to a maximum radial distance of 5 mm. More specifically, we used each volume and the corresponding tumor core mask to generate the peritumoral masks via morphological image processing operations. The calculation procedure of PTV is described in Algorithm 1. A schematic diagram of the different sizes of PTVs is shown in Fig 3. Therefore, there are five PTVs in conjunction with the peritumoral edema (PED) mentioned above that are considered for evaluation to find the optimal peritumoral radiomic signature.

2.3 Extraction of radiomic features

The feature extraction of VOIs is critical in radiomics and determines whether important biomarkers can be found. In this study, both intratumoral and peritumoral radiomic features were extracted using the PyRadiomics toolbox [35], an open-source python software package for extracting radiomic features from medical images. For the features extracted from PTVs, we first developed the preprocessing program for the peritumoral masks as described in Algorithm 1 and seamlessly embedded it into the PyRadiomics toolbox. To mine rich and valuable radiomic features, we first preprocessed each intratumoral and peritumoral VOI on each MRI image using the methods based on six intensity transformations (i.e., original no filtering, square filtering, square root filtering, logarithm filtering, exponential filtering and gradient filtering), Laplacian of Gaussian (LoG) filters with five different sigma values, wavelet filters with eight decompositions, and local binary pattern (LBP) filters with four settings [42], [43]. Then, we quantified the features by the following seven feature categories: features based on first order statistics (19 features), 2D and 3D Shape (26 features), Gray Level Co-occurrence Matrix (GLCM, 24 features), Gray Level Run Length Matrix (GLRLM, 16 features), Gray Level Size Zone Matrix (GLSZM, 16 features), Neighboring Gray Tone Difference Matrix (NGTDM, 5 features) and Gray Level Dependence Matrix (GLDM, 14 features). The detailed radiomics extraction methodology can be found at https://pyradiomics.readthedocs.io/en/latest/. Eventually, 2153 quantitative radiomic features were extracted from each VOI. A schematic diagram of the features extracted from each VOI is shown in Fig. 1B.

2.4 Feature selection and classifier modeling

For intratumoral and peritumoral radiomics features, we first normalized all features by subtracting the mean and scaling to unit variance, which is beneficial to make the range of each feature relatively uniform and avoid assigning a lower or greater weight to some features. This method is referred to as z-score normalization and can be found in other works [13], [23]. Then, we removed the features where the variance is close to zero in the training data.

For the intratumoral radiomics study, we first used the least absolute shrinkage and selection operator (LASSO) regression method which has been proven to be suitable for the regression of high-dimensional data [44] to select the most useful and predictive combination of features for each modality. The LASSO mathematically consists of a

linear model with the $\ell 1$-norm, and its objective function is defined by (1). The optimal parameter configuration in LASSO is determined using the smallest error in five-fold cross-validation on the training data. After $L1$ regularization, the coefficients of most radiomic features are equal to zero, and the remaining nonzero coefficient radiomic features are used as the optimal combination of features. However, for multimodality, we first fused the optimal features from each modality and then used the minimum redundancy maximum relevance (mRMR) algorithm [45] to eliminate redundant features. The mRMR finds the optimal feature combination by encouraging maximum relevance while removing minimum redundant features, which can be described by (2).

$$\mathcal{L} = \min_{w} \frac{1}{2m} ||Xw - y||_2^2 + \alpha ||w||_1, \tag{1}$$

$$\Phi(X, c) = \max \left[\frac{1}{|X|} \sum_{x_i \in X, c \in y} I(x_i; c) - \frac{1}{|X|^2} \sum_{x_i, x_j \in X} I(x_i, x_j) \right], \tag{2}$$

where m is the number of samples, α is a constant and $||w||_1$ is the $\ell 1$-norm of the coefficient vector. X indicates the total feature set, y is the category of glioma grade, I represents mutual information, x_i and x_j are the individual features.

Then, the top-ranking radiomic features were entered into the classifiers to build radiomic signatures for predicting glioma grade. To reduce overfitting, we used five-fold cross-validation on a patient-level split to randomly divide the dataset into five subsets, four of which were used for training the classifiers, and the remaining subset was used for testing. Due to our imbalanced data, a synthetic minority oversampling technique (SMOTE) [46] was adopted in the training data to generate synthetic samples from the LGG category and obtain a synthetically class-balanced or nearly class-balanced training set, which is beneficial for model building. The classifiers were trained only using the training fold, and the testing fold was used to evaluate their performance. To investigate the effectiveness of the selected features, four classifiers, namely, logistic regression (LR) [47], support vector machine (SVM) [48], random forest (RF) [49] and XGBoost (XGB) [50], were adopted in this study. Radiomic signatures based on ITVs and PTVs were built on different VOIs and modalities. In addition, the optimal intratumoral and peritumoral radiomic features on multimodality were combined together to generate an intratumoral and peritumoral volume (IPTV) radiomic signature using the same method mentioned above.

2.5 Performance evaluation

To fairly evaluate the predictive performance of the radiomic signatures, we performed the glioma grading experiments on mpMRI images using intratumoral, peritumoral and combined radiomic features, respectively. Receiver operating characteristic (ROC) curve analysis was performed, and the area under the curve (AUC) value of the ROC curve was calculated to evaluate the predictive performance of the models. Accuracy, sensitivity, and specificity metrics were also used to measure the performance and are computed by (3-5), respectively. In particular, the positive case in our experiment is HGG. Since we use five-fold cross-validation in this study, the procedures of feature selection, classifier modeling and model evaluation are performed five times. Thus, the results on all metrics we report are presented by an average value of five sets of measures.

$$Accuracy = \frac{TP + TN}{TP + FP + TN + FN}, \tag{3}$$

$$Sensitivity = \frac{TP}{TP + FP}, \tag{4}$$

$$Specificity = \frac{TN}{TN + FP}, \tag{5}$$

where TP is true positives, FP is false positives, TN is true negatives and FN is false negatives.

3 Experiments and Results

In this section, we will perform three experiments on the BraTS 2017 dataset to evaluate the predictive performance

TABLE 2: The average performance results of nonenhancing tumor volumes on each MRI scan using various classifiers.

Scan	Classifier	AUC	Accuracy	Specificity	Sensitivity
FLAIR	LR	0.938	0.874	0.851	0.881
	RF	**0.948**	**0.919**	**0.851**	**0.943**
	SVM	0.926	0.863	0.819	0.876
	XGB	0.937	0.881	0.782	0.915
T1	LR	0.939	0.870	0.785	0.895
	RF	**0.956**	**0.916**	**0.842**	**0.943**
	SVM	0.925	0.870	0.763	0.905
	XGB	0.943	0.898	0.819	0.927
T1Gd	LR	0.955	0.902	**0.851**	0.921
	RF	**0.958**	0.916	0.823	0.947
	SVM	0.956	0.902	0.834	0.926
	XGB	0.957	**0.923**	0.840	**0.952**
T2	LR	0.945	0.891	**0.854**	0.903
	RF	**0.955**	**0.916**	0.817	**0.953**
	SVM	0.935	0.877	0.819	0.893
	XGB	0.953	0.905	0.797	0.944

TABLE 3: The average performance results of tumor core volumes on each MRI scan using various classifiers.

Scan	Classifier	AUC	Accuracy	Specificity	Sensitivity
FLAIR	LR	0.836	0.779	0.713	0.803
	RF	0.852	0.790	0.642	0.841
	SVM	0.837	0.754	**0.721**	0.777
	XGB	**0.855**	**0.807**	0.698	**0.845**
T1	LR	0.741	0.716	**0.591**	0.769
	RF	**0.791**	**0.751**	0.514	0.825
	SVM	0.740	0.729	0.562	**0.845**
	XGB	0.781	0.726	0.503	0.799
T1Gd	LR	0.914	0.888	0.778	0.922
	RF	**0.937**	0.888	0.769	**0.927**
	SVM	0.899	0.870	0.749	0.907
	XGB	0.925	**0.898**	**0.827**	0.921
T2	LR	0.858	0.814	0.743	0.842
	RF	**0.894**	**0.849**	0.732	**0.887**
	SVM	0.851	0.800	0.685	0.842
	XGB	0.888	0.832	**0.743**	0.866

of glioma grading on mpMRI images, compare our studies with five other state-of-the-art approaches, and then verify the generalization performance using an external validation dataset. Our whole experimental procedure was implemented on an Intel (R) Core (TM) 16.0 GB RAM CPU @ 3.2.0 GHz processor with a 64-bit operating system, and the software environment is based on Python 3.6 (https://www.python.org).

3.1 Intratumoral radiomics to discriminate glioma grade

For a single MRI scan, the significant radiomic features chosen from the LASSO feature selection algorithm on each fold were used to build radiomic signatures using four classifiers. Tables 2 and 3 list the AUC and other measurements of the four classifiers of nonenhancing tumor and tumor core volumes in each MRI scan, respectively. We can see that the study of nonenhancing tumors on each modality can better distinguish glioma grade compared to the tumor core volume, and random forest performs better than the other three classifiers with respect to most measurements. Moreover, the performance of each classifier on the T1Gd scan is almost better than that of the other MRI scans, which means that the glioma grading can be identified with higher accuracy from the T1Gd scan.

To further improve the prediction accuracy, glioma grading based on mpMRI scans was performed. The top 20 radiomic features produced by the mRMR algorithm from the above significant radiomic features on each MRI scan were used to build a mpMRI scan-based radiomic signature. Tables A.1 and A.2 present the most important radiomic features in nonenhancing tumor and tumor core volumes, respectively. These important features appear at least three times in five-fold cross-validation. In the nonenhancing tumor study, the gray level nonuniformity normalized (GLNN) feature of GLSZM processed by the 3D LBP filter, which indicates the variability of gray-level intensity values in the image, is frequently represented among the mpMRI scans. The next most efficacious features are the dependence variance of the GLDM processed by the exponential filter and the mean of the first-order processed by the 2D LBP filter. However, for the tumor core, one of the most important features is the skewness of the first-order processed by the square filter, which measures the asymmetry of the distribution of voxels about the mean voxels. Other significant features are listed in Table A.2.

TABLE 4: The average performance results of nonenhancing tumor and tumor core volumes on mpMRI scans using various classifiers.

VOI	Classifier	AUC	Accuracy	Specificity	Sensitivity
NET	LR	0.948	0.895	**0.885**	0.902
	RF	**0.968**	**0.930**	0.856	**0.958**
	SVM	0.947	0.881	0.817	0.911
	XGB	0.963	0.930	0.866	0.953
TC	LR	0.909	0.860	0.801	0.881
	RF	**0.943**	**0.891**	**0.805**	**0.924**
	SVM	0.906	0.863	0.792	0.890
	XGB	0.937	0.863	0.720	0.915

By using the top 20 features in each fold, the highest average AUC of 0.968 in five-fold cross-validation is obtained by using the random forest classifier on nonenhancing tumors. The other performance metrics were an accuracy of 93.0%, a specificity of 85.6%, and a sensitivity of 95.6%. However, for the tumor core, its best performance is not as good as that of the nonenhancing tumor. Table 4 lists the performance metrics of the other classifiers on both nonenhancing tumor and tumor core volumes. Fig. 4 displays the mean receiver operating of characteristic curves and the distribution of radiomic signature scores for nonenhancing tumor and tumor core volumes. The Fig. 4c and Fig. 4d illustrate that the denseness of the signature score in the nonenhancing tumor is better than that in the tumor core. Therefore, the radiomic features from the nonenhancing tumor are more predictive than that from the tumor core and can be used as imaging biomarkers of glioma grading in intratumoral radiomics.

3.2 Peritumoral radiomics to discriminate glioma grade

In the peritumoral radiomics studies, the most predictive features based on mpMRI scans were found to be within an immediate distance of 1 mm from the tumor core. The random forest classifier also reached the highest AUC of 0.968 in five-fold cross-validation, which suggests that the peritumoral microenvironment is as essential as the intratumoral nonenhancing tumor for grading gliomas. Table 5 shows the quantitative results of five peritumoral volumes in conjunction with peritumoral edema and Fig. 5 presents the corresponding trend curves of each classifier in all measurements.

TABLE 5: The average performance results of the PTVs and PED radiomic signatures on mpMRI scans using various classifiers.

VOI	Classifier	AUC	Accuracy	Specificity	Sensitivity
1 mm	LR	0.929	0.895	0.833	0.920
	RF	**0.968**	**0.919**	0.862	**0.942**
	SVM	0.930	0.898	0.814	0.930
	XGB	0.962	0.916	**0.867**	0.937
2 mm	LR	0.930	0.895	0.827	0.924
	RF	0.951	0.909	0.835	0.938
	SVM	0.924	0.891	0.777	0.937
	XGB	0.953	0.912	0.848	0.937
3 mm	LR	0.947	0.898	0.853	0.920
	RF	0.945	0.902	0.822	0.933
	SVM	0.942	0.891	0.830	0.921
	XGB	0.938	0.888	0.781	0.928
4 mm	LR	0.893	0.821	0.803	0.828
	RF	0.892	0.814	0.785	0.827
	SVM	0.894	0.825	0.831	0.821
	XGB	0.888	0.828	0.847	0.860
5 mm	LR	0.891	0.772	0.820	0.746
	RF	0.865	0.786	0.720	0.801
	SVM	0.891	0.772	0.820	0.745
	XGB	0.873	0.839	0.743	0.867
PED	LR	0.921	0.873	0.816	0.890
	RF	0.935	0.894	0.777	0.929
	SVM	0.923	0.870	0.774	0.900
	XGB	0.933	0.898	0.805	0.922

As shown in Table 5 and Fig. 5, both the logistic regression and support vector machine classifiers have similar trends in all measurements, achieving a better performance at 3 mm. However, the best diagnostic performance of the two classifiers based on ensemble learning, random forest and XGBoost achieved AUCs of 0.968 and 0.962 at 1 mm, respectively. The performance of both two peritumoral volumes ($1mm$ and $3mm$) is better than that of peritumoral edema. Table A.3 lists the most important radiomic features appearing at least three times from five-fold cross-validation in the peritumoral volume within 1 mm. In FLAIR and T2 scans, the gray level nonuniformity (GLN) of GLSZM preprocessed by an exponential filter reflects the strong similarity of gray-level intensity values in the glioma grade category. Meanwhile, the features preprocessed by the 3D LBP filter are frequently represented in T1Gd scans, which means that LBP is an effective method for feature mining and can be found in brain tumor detection [51].

3.3 Combined intratumoral and peritumoral radiomics to distinguish glioma grade

To improve the predictive performance, we further investigated the diagnostic ability of predicting glioma grade by combining intratumoral and peritumoral radiomics. More precisely, the features from mpMRI scans in intratumoral nonenhancing tumor and peritumoral 1 mm volumes were used to build an IPTV radiomic signature. Likewise, the top 20 radiomic features produced by the mRMR algorithm in each fold and the most important nine features from five folds are listed in Table A.4. Of these features, five are from the intratumoral volume, three from the peritumoral volume, and one is from both the intratumoral and peritumoral volumes. The features based on the 3D LBP filter dominate all the selected important features, as do the features extracted from the T1Gd scan.

Table 6 shows the quantitative results of the IPTV radiomic signatures on mpMRI scans using various classifiers. Fig. 6 displays the corresponding mean receiver operating of characteristic curves and the distribution of IPTV radiomic signature scores between the HGG and LGG gloups. Fig. 7 presents a histogram of the AUC of each classifier of intratumoral nonenhancing tumor volume, peritumoral 1 mm volume, and their combination. The quantitative results and visual analysis show that the performance of the IPTV radiomic signatures is better than that of the individuals in each classifier. Generally, the ensemble learning-based classifiers (RF and XGB) outperform the linear-based classifiers (LR and SVM) in terms of most measurements. Although the random forest classifier is comparable to the XGBoost classifier in terms of accuracy and specificity, it achieves the best AUC with a value of 0.975. The other improvements were an accuracy of 94.0%, a specificity of 87.1% and a sensitivity of 96.7%.

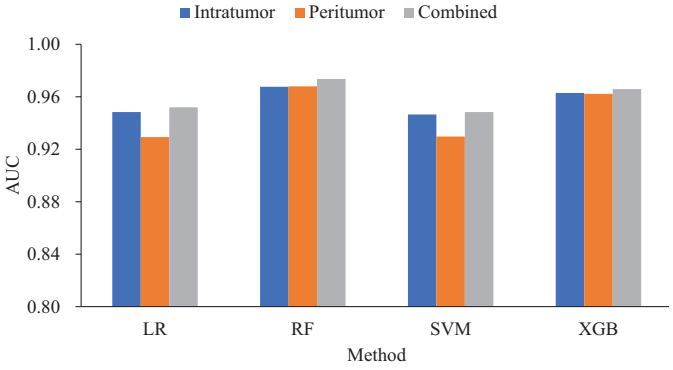

Fig. 7: Histogram of the AUC of each method for the intratumoral volume, peritumoral volume and their combination.

TABLE 6: The average performance results of the IPTV radiomic signatures on mpMRI scans using various classifiers.

Region	Classifier	AUC	Accuracy	Specificity	Sensitivity
NET+1mm	LR	0.952	0.898	0.892	0.901
	RF	**0.975**	**0.940**	0.871	**0.967**
	SVM	0.948	0.888	**0.901**	0.885
	XGB	0.966	0.940	0.871	0.965

3.4 Comparison with other works

To verify the superiority of our studies, we compared our works with the other state-of-the-art works [12], [13], [27], [52], [53] based on radiomics in the last two years. Since the works [12], [13], [27] are based on the same dataset, their results are referred to directly. Moreover, we implemented the experimental procedures in references [52] and [53] based on the BraTS 2017 training dataset. The comparison results are listed in Table 7 and our results are shown in the last three rows. Notably, the performance of our work based on intratumoral radiomics significantly outperforms that of the other works, which shows that nonenhancing tumors in intratumoral volume have a better ability to distinguish high-grade gliomas from low-grade gliomas than other VOIs. Our work based on peritumoral radiomics has also shown competitive results. More importantly, the combination with intratumoral and peritumoral radiomics achieves the state-of-the-art performance.

TABLE 7: Experimental results of the other state-of-the-art comparison approaches and our proposed methods on the BraTS 2017 dataset.

Method	AUC	Accuracy	Specificity	Sensitivity
Reza et al. [12]	0.880	0.880	0.620	0.980
Cho et al. [13]	0.921	0.888	0.733	0.943
Xiao et al. [27]	0.942	0.909	0.827	0.929
Bi et al. [52]	0.915	0.884	0.804	0.911
Cui et al. [53]	0.934	0.884	0.739	0.940
Intratumoral Radiomics **(this study)**	0.968	0.930	0.856	0.958
Peritumoral Radiomics **(this study)**	0.968	0.919	0.862	0.942
Intra- and Peritumoral Radiomics **(this study)**	0.975	0.940	0.871	0.967

3.5 External validation

To further validate our methods, we performed the external validation experiments based on 65 patients mentioned in Section 2. More specifically, we used BraTS 2017 dataset as

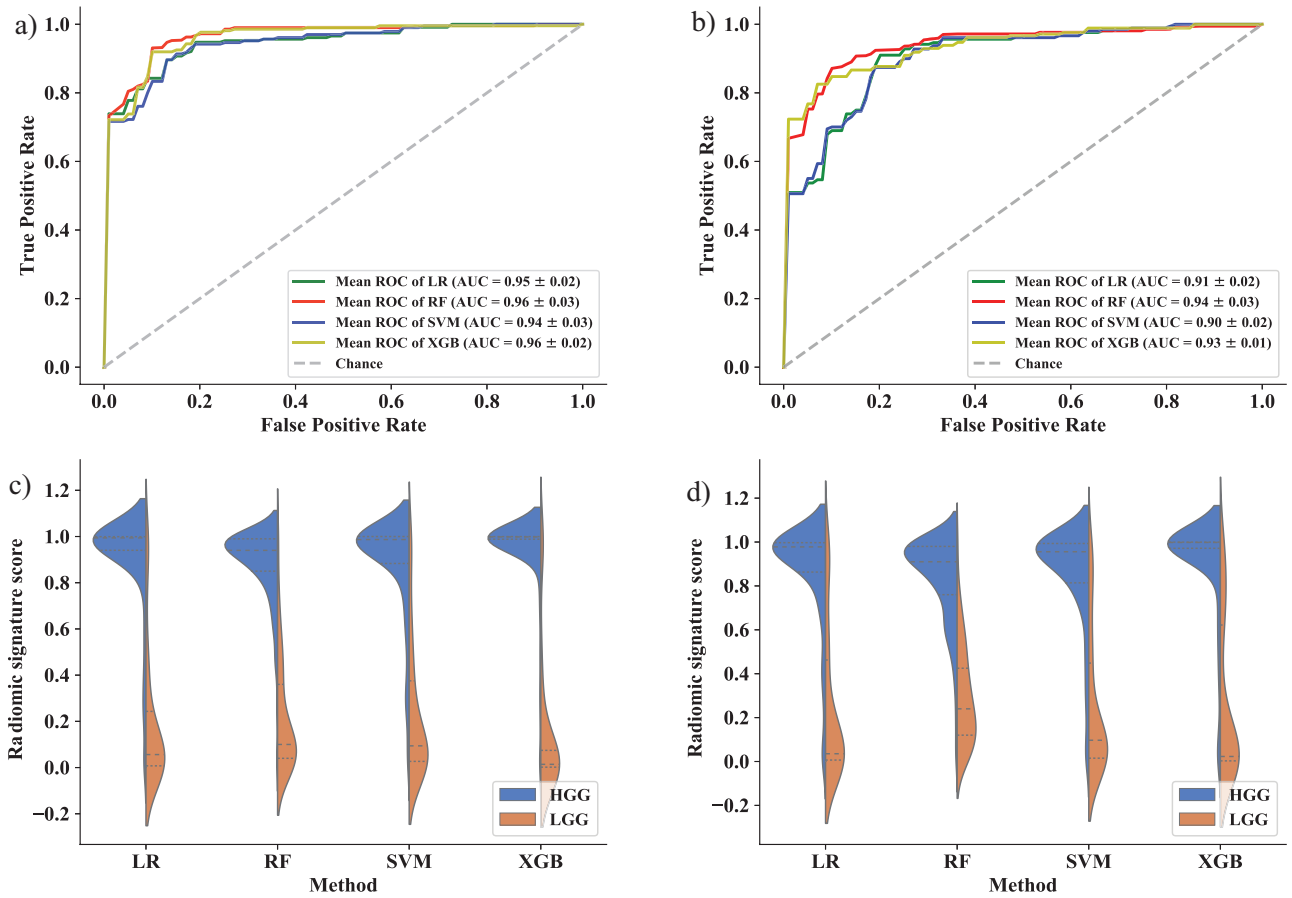

Fig. 4: Predictive performance of the ITV radiomic signature using five-fold cross-validation on mpMRI scans. a) and b) are the mean receiver operating characteristic curves of the nonenhancing tumor and tumor core volumes, respectively. c) and d) are the radiomic signature scores between the HGG and LGG gloups of nonenhancing tumor and tumor core volumes, respectively.

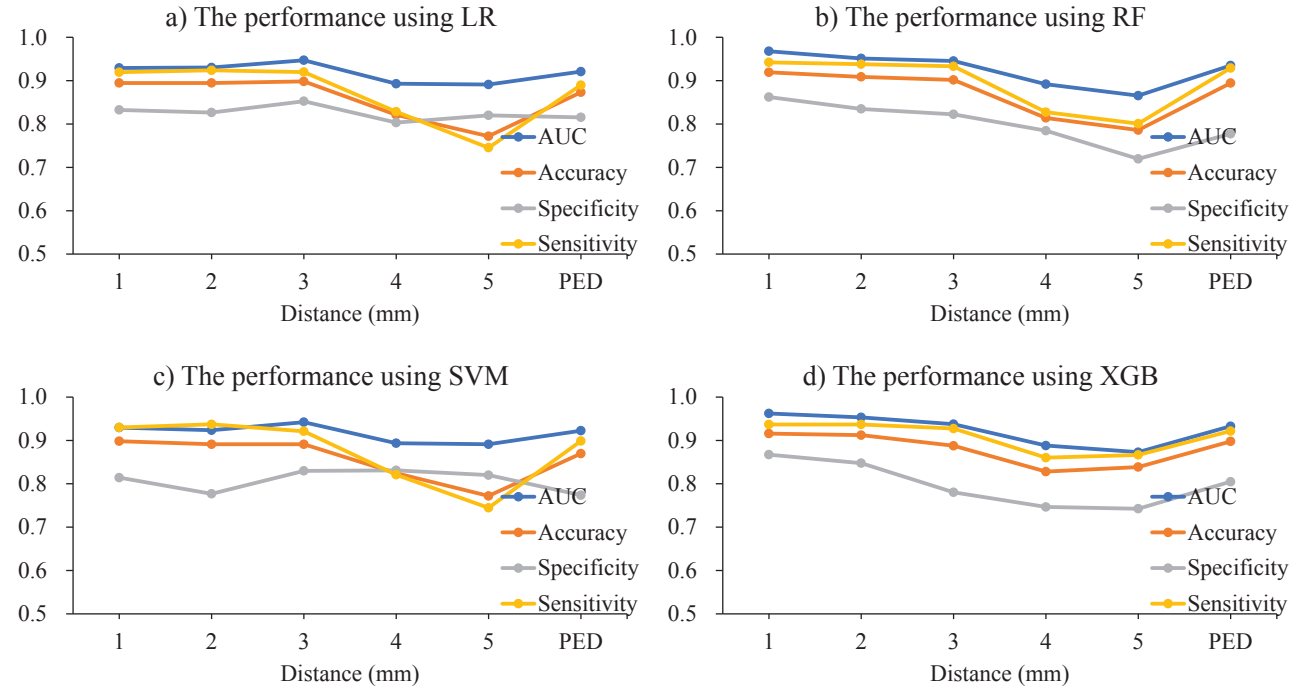

Fig. 5: Comparison of performance using various methods for five PTVs in conjunction with PED.

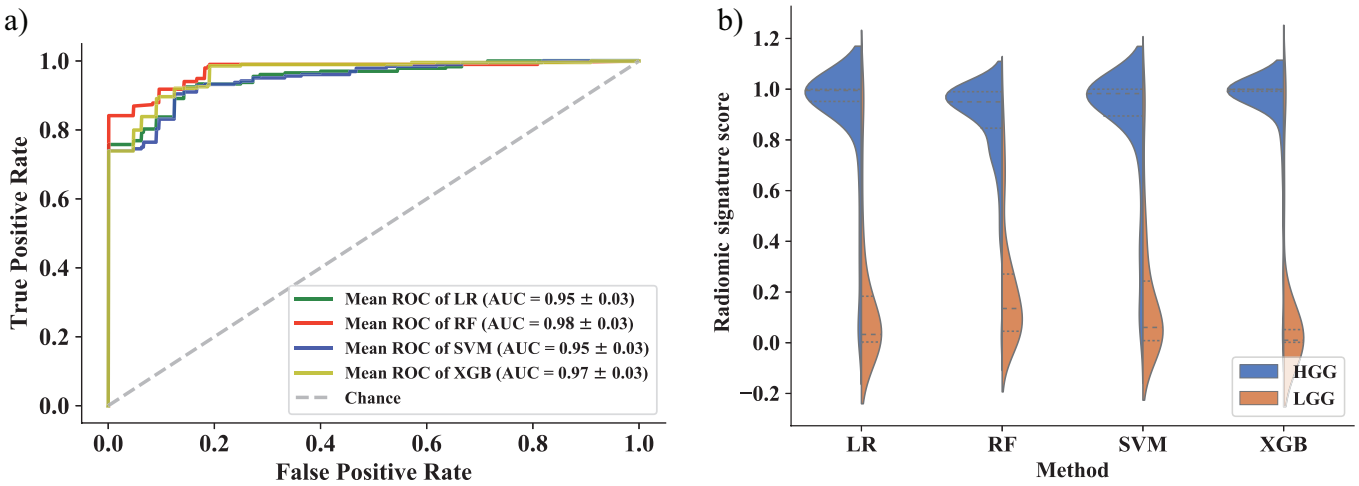

Fig. 6: Predictive performance of the IPTV radiomic signature using five-fold cross-validation on mpMRI scans. a) The mean receiver operating characteristic curves of combining with nonenhancing tumor and peritumoral 1 mm volumes. b) The IPTV radiomic signature score between the HGG and LGG groups combined with nonenhancing tumor and peritumoral 1 mm volumes.

the training set, chose random forest as the classifier, and build ITV, PTV and IPTV radiomic signatures based on their respective imaging biomarkers (see Tables A.1, A.3 and A.4). Then, we used 65 patients as a testing set to validate the performance of three radiomic signatures. The validation results of three radiomic signatures are presented in Table 8. The results show that the performance of ITV radiomic signature is better than that of PTV radiomic signature in terms of all measurements. By combining intratumoral and peritumoral radiomic features, IPTV radiomic signature achieves a better predictive performance with an accuracy of 95.4%, a specificity of 82.4%, and a sensitivity of 100%. It is noticed that although the AUC of the IPTV radiomic signature is more moderate than that of the ITV radiomic signature, IPTV radiomic signature has better accuracy, specificity and sensitivity. Therefore, our proposed IPTV radiomic signature has a strong generalization performance.

TABLE 8: Experimental results of three radiomic signatures on external validation dataset.

Signature	Accuracy	Specificity	Sensitivity	AUC
ITV	0.923	0.765	0.979	0.961
PTV	0.877	0.765	0.917	0.856
IPTV	0.954	0.824	1.000	0.933

4 Discussion

As an integral part of treatment options, personalized therapy, and prognosis prediction, accurate glioma grading from preoperative mpMRI scans, which is noninvasive and inexpensive, has attracted the attention of medical workers and researchers. They have focused on radiomics since 2012 [54], which has emerged as a promising machine learning method to extract biomarkers from medical images for grading gliomas. Most of the prior investigations involving intratumoral radiomics focus on the whole tumor, tumor core and enhancing tumor region, but their prediction accuracy remains to be improved. In this study, we investigated the ability of radiomic features extracted from the nonenhancing tumor and peritumoral volumes of glioma on preoperative mpMRI scans to distinguish high-grade gliomas from low-grade gliomas.

We found that the intratumoral nonenhancing tumor plays an important role in predicting glioma grade and that its predictive performance exceeds that of other parts of the intratumoral area. Clinical studies have also shown that nonenhancing tumors are highly associated with the overall survival and prognosis of patients [14], [16]. Therefore, the intratumoral radiomic features from nonenhancing tumors may be used as imaging biomarkers for grading gliomas. Notably, the gray level nonuniformity normalized feature of the 3D LBP filter is frequently represented among the mpMRI scans, which indicates that there is a greater difference in gray-level intensity values between the high-grade gliomas and low-grade gliomas on mpMRI scans after processing by the 3D LBP filter. The dependence variance measures the variance in gray level dependence size in mpMRI images. This feature from the T1Gd scan preprocessed by an exponential filter plays an important role in predicting glioma grade. The mean feature of the first-order from the T1Gd preprocessed by the 2D LBP filter is the average gray level intensity within the nonenhancing tumor volumes, which is also critical to glioma grading. Other features from nonenhancing tumor region that play a positive role in predicting glioma grade can be found in Table A.1.

Another important contribution is that we designed an algorithm to quantitatively calculate features from the peritumoral region with unclear boundaries. We found that the classifiers have a highly predictive performance for grading gliomas in the immediate vicinity of 1 mm up to 3 mm outside the tumor core (see Table 5). Especially in the immediate vicinity of 1 mm, the best predictive performance is

comparable to that of the intratumoral nonenhancing tumor in terms of the AUC, with a value of 0.968 (see Tables 4 and 5). Similarly, imaging biomarkers based on 3D LBP filters also occur at high frequencies. The correlation features based on square and wavelet filters from T1Gd show the linear dependency of gray level values on their respective voxels in the GLCM. Most notably, we incorporated the most important radiomic features in the intratumoral and peritumoral volumes, and the best predictive ability of the IPTV signature reached an average AUC of 0.975, compared with an AUC of 0.968 for ITV (nonenhancing tumor volumes) and PTV (peritumoral 1 mm volumes) alone (see Tables 4, 5 and 6).

The majority of radiomic methods used in grading gliomas have focused solely on whole tumor or tumor core texture analysis and shape features from preoperative mpMRI scans [10], [11], [12], [13], [27], [52], [53]. To specifically distinguish high-grade gliomas from low-grade gliomas, a study used radiomic features from conventional MRI scans and advanced images (such as DWI, DTI, DSCE, and 1H-MRS, etc) to build a radiomic signature, which achieved an AUC of 0.955 [11]. However, their study utilized only 40 patients from a single site, and their conclusion could be potentially biased. Another study used an intratumoral radiomics-based method with molecular features to obtain an accuracy improvement from 0.83 to 0.86 in the TCIA dataset [12]. Cho et al reported that shape-based feature (such as spherical disproportion, compactness) from the intratumoral region were important for determining glioma grade, and their radiomic signature achieved a high sensitivity of 0.943 but had a low specificity of 0.733 [13]. Unlike previously reported features [13], our radiomic feature selection method does not choose shape-based features, but chooses first-order and texture features in our studies, suggesting that these radiomic features have a more predictive performance in grading gliomas than the shape-based features. Moreover, we used an external validation dataset to further validate and evaluate the performance based on the important radiomic features shown in Table A.4. The IPTV radiomic signature achieves a strong generalization performance with an AUC of 93.3%, an accuracy of 95.4%, a specificity of 82.4%, and a sensitivity of 100% (see Table 8). This result further demonstrates that the radiomic features we report have a strong predictive performance and can be used as imaging biomarkers to distinguish glioma grade.

The majority of deep learning-based methods [29], [30] also have strong predictive performance and are comparable to the traditional radiomics-based approaches, but these methods have limited ability to explain the deep features with neither a set of diagnostic plans nor an insight into the results [55]. Although the deep learning approaches are still difficult to convince, their superiority and predictive performance are amazing. These methods do not require the doctor or radiologist to specify a priori features but can implicitly learn the abstract features associated with the problem of radiomics research. Compared with traditional radiomic methods, deep learning usually requires a large number of training samples to train a model with many hyperparameters. We intend to undertake this promising and meaningful research in our next work.

Although our study provides insights into the application of radiomics in computer-aided diagnosis, this study has several limitations. Firstly, our research was based on two public datasets derived from a multi-institutional segmentation task, which may have a certain bias in selecting patients. In future work, independent validation data from multiple sources will be used to verify whether the radiomic signature can be generalized to other institutions. Secondly, the feature selection scheme used in this study is a standalone procedure for the following classifier learning, which may lead to the suboptimal problem. The embedded feature selection method and more advanced method such as disentangled representation [56] will be studied in the future, because they can simultaneously integrate modeling with feature selection for a better coordination. Thirdly, only four MRI scans were used in this study. Some advanced parametric MRI scans (such as DTI [11] and ADC [57]), histology images, and genomic data have shown strong potential in glioma studies, but the combination of these data is unclear. Finally, our study only focused on the classification of high- and low-grade glioma. Future studies should explore more advanced methods for the relationship between tumor grades (WHO grades I-IV) and other genetic mutations ($e.g.$, IDH mutation [58], 1p/19q codeletion [59]) based on multisource heterogeneous data.

5 Conclusion

In conclusion, we proposed a novel radiomics-based method that uses the radiomic features extracted separately from the intratumoral nonenhancing tumor volumes and peritumoral volumes on preoperative mpMRI scans to accurately and noninvasively predict glioma grade. Our proposed method was evaluated and validated on the BraTS 2017 dataset and an external validation dataset. Quantitative results show that combining intratumoral features with peritumoral features can improve the predictive ability of the classifier to differentiate glioma grade and may play a greater role in computer-aided diagnosis.

Appendix A
Significant radiomic features

Acknowledgments

This work is supported in part by the National Natural Science Foundation of China under Grant No.61802442, No.61877059, the Natural Science Foundation of Hunan Province under Grant No.2019JJ50775, the 111 Project (No. B18059), and the Hunan Provincial Science and Technology Program (2018WK4001).

References

[1] G. S Tandel, M. Biswas, O. G Kakde, A. Tiwari, H. S Suri, M. Turk, J. R. Laird, C. K. Asare, A. A Ankrah, N. N Khanna *et al.*, "A review on a deep learning perspective in brain cancer classification," *Cancers*, vol. 11, no. 1, p. 111, 2019.

[2] D. N. Louis, H. Ohgaki, O. D. Wiestler, W. K. Cavenee, P. C. Burger, A. Jouvet, B. W. Scheithauer, and P. Kleihues, "The 2007 who classification of tumours of the central nervous system," *Acta neuropathologica*, vol. 114, no. 2, pp. 97–109, 2007.

[3] L. Qin, A. Li, J. Qu, K. Reinshagen, X. Li, S.-C. Cheng, A. Bryant, and G. S. Young, "Normalization of adc does not improve correlation with overall survival in patients with high-grade glioma (hgg)," *Journal of neuro-oncology*, vol. 137, no. 2, pp. 313–319, 2018.

TABLE A.1: Significant radiomic features from five-fold cross-validation in the nonenhancing tumor volumes.

No.	Feature name	Times	Modality
1	lbp-3D-k_glszm_GrayLevelNon UniformityNormalized	10	T1Gd(2)*,T2(3)*, FLAIR(4)*,T1(1)*
2	exponential_gldm_Dependence Variance	5	T1Gd(4)*,T1(1)*
3	lbp-2D_firstorder_Mean	5	T1Gd
4	lbp-3D-k_gldm_DependenceNon UniformityNormalized	4	T2
5	log-sigma-1-0-mm-3D_firstorder _Skewness	4	T1Gd
6	square_glcm_Imc1	4	T1Gd
7	exponential_glrlm_LongRunLow GrayLevelEmphasis	3	T1Gd
8	lbp-3D-k_glcm_Imc1	3	T2
9	log-sigma-1-0-mm-3D_firstorder _Kurtosis	3	T2
10	log-sigma-5-0-mm-3D_firstorder _Skewness	3	T2
11	wavelet-HLH_glszm_SmallArea Emphasis	3	T2
12	wavelet-HLH_glcm_Correlation	3	T1

* Represents the number of times a feature is repeatedly appeared.

TABLE A.2: Significant radiomic features from five-fold cross-validation in the tumor core volumes.

No.	Feature name	Times	Modality
1	square_firstorder_Skewness	5	T2(3)*, FLAIR(2)*
2	wavelet-LHL_glcm_Correlation	5	T1Gd
3	exponential_glrlm_ShortRunLow GrayLevelEmphasis	4	FLAIR
4	wavelet-LHL_gldm_LargeDepend enceHighGrayLevelEmphasis	4	T2
5	wavelet-LLH_glcm_Correlation	4	T1Gd
6	exponential_gldm_DependenceVariance	4	T1Gd
7	lbp-2D_firstorder_Kurtosis	4	T2
8	lbp-3D-m1_firstorder_Skewness	3	FLAIR
9	lbp-2D_firstorder_Mean	3	T1Gd(2)*,T2(1) *

* Represents the number of times a feature is repeatedly appeared.

TABLE A.3: Significant radiomic features from five-fold cross-validation in the peritumoral volumes within 1 mm.

No.	Feature name	Times	Modality
1	exponential_glszm_GrayLevel NonUniformity	6	FLAIR(4)*, T2(2)*
2	lbp-3D-m1_firstorder_Skewness	5	T1Gd
3	square_glcm_Correlation	5	T1Gd
4	lbp-3D-k_glszm_SizeZoneNon UniformityNormalized	4	T1Gd
5	lbp-3D-m1_firstorder_Mean	4	FLAIR(1)*, T1Gd(3)*
6	wavelet-LLL_glcm_Correlation	4	T1Gd
7	lbp-3D-k_glrlm_RunEntropy	4	T1Gd
8	lbp-3D-m2_firstorder_90Percentile	4	T2
9	wavelet-HLL_firstorder_Median	3	T1Gd
10	lbp-3D-k_glcm_Imc1	3	T2

* Represents the number of times a feature is repeatedly appeared.

TABLE A.4: Significant radiomic features from five-fold cross-validation in the peritumoral and intratumoral volumes.

No.	Feature name	Times	Modality	VOI
1	lbp-3D-k_glszm_GrayLevel NonUniformityNormalized	5	FLAIR,T1, T1Gd(2)*,T2	Intratumor
2	lbp-3D-m1_firstorder_Skewness	5	T1Gd	Peritumor
3	lbp-3D-k_glrlm_RunEntropy	4	T1Gd	Peritumor
4	square_glcm_Imc1	4	T1Gd	Intratumor
5	lbp-2D_firstorder_Mean	4	T1Gd	Intratumor
6	wavelet-LLL_glcm_Correlation	3	T1Gd	Peritumor
7	lbp-3D-k_gldm_Dependence NonUniformityNormalized	3	T2	Intratumor
8	exponential_gldm_Depen denceVariance	3	T1Gd	Intratumor
9	lbp-3D-k_glcm_Imc1	3	T2	Intratumor(2)†, Peritumor(1)†

* Represents the number of times a feature is repeatedly appeared.
† Represents the number of times a feature is repeatedly appeared.

[4] D. Nie, J. Lu, H. Zhang, E. Adeli, J. Wang, Z. Yu, L. Liu, Q. Wang, J. Wu, and D. Shen, "Multi-channel 3d deep feature learning for survival time prediction of brain tumor patients using multi-modal neuroimages," *Scientific reports*, vol. 9, no. 1, p. 1103, 2019.

[5] J. Cheng, J. Liu, L. Liu, Y. Pan, and J. Wang, "Multi-level glioma segmentation using 3d u-net combined attention mechanism with atrous convolution," in *2019 IEEE International Conference on Bioinformatics and Biomedicine (BIBM)*, 2019, pp. 1031–1036.

[6] J. Liu, J. Wang, Z. Tang, B. Hu, F.-X. Wu, and Y. Pan, "Improving alzheimer's disease classification by combining multiple measures," *IEEE/ACM transactions on computational biology and bioinformatics*, vol. 15, no. 5, pp. 1649–1659, 2018.

[7] J. E. Villanueva-Meyer, M. C. Mabray, and S. Cha, "Current clinical brain tumor imaging," *Neurosurgery*, vol. 81, no. 3, pp. 397–415, 2017.

[8] J. Liu, Y. Pan, F.-X. Wu, and J. Wang, "Enhancing the feature representation of multi-modal mri data by combining multi-view information for mci classification," *Neurocomputing*, vol. 400, pp. 322 – 332, 2020.

[9] J. Liu, Y. Pan, M. Li, Z. Chen, L. Tang, C. Lu, and J. Wang, "Applications of deep learning to mri images: A survey," *Big Data Mining and Analytics*, vol. 1, no. 1, pp. 1–18, 2018.

[10] E. I. Zacharaki, S. Wang, S. Chawla, D. S. Yoo, R. Wolf, E. R. Melhem, and C. Davatzikos, "Mri-based classification of brain tumor type and grade using svm-rfe," in *2009 IEEE International Symposium on Biomedical Imaging: From Nano to Macro*. IEEE, 2009, pp. 1035–1038.

[11] A. Vamvakas, S. Williams, K. Theodorou, E. Kapsalaki, K. Fountas, C. Kappas, K. Vassiou, and I. Tsougos, "Imaging biomarker analysis of advanced multiparametric mri for glioma grading," *Physica Medica*, vol. 60, pp. 188–198, 2019.

[12] S. M. Reza, M. D. Samad, Z. A. Shboul, K. A. Jones, and K. M. Iftekharuddin, "Glioma grading using structural magnetic resonance imaging and molecular data," *Journal of Medical Imaging*, vol. 6, no. 2, p. 024501, 2019.

[13] H.-h. Cho, S.-h. Lee, J. Kim, and H. Park, "Classification of the glioma grading using radiomics analysis," *PeerJ*, vol. 6, p. e5982, 2018.

[14] A. Kotrotsou, A. Elakkad, J. Sun, G. A. Thomas, D. Yang, S. Abrol, W. Wei, J. S. Weinberg, A. S. Bakhtiari, M. F. Kircher *et al.*, "Multi-center study finds postoperative residual non-enhancing component of glioblastoma as a new determinant of patient outcome," *Journal of neuro-oncology*, vol. 139, no. 1, pp. 125–133, 2018.

[15] A. Lasocki and F. Gaillard, "Non-contrast-enhancing tumor: a new frontier in glioblastoma research," *American Journal of Neuroradiology*, vol. 40, no. 5, pp. 758–765, 2019.

[16] R. Jain, L. M. Poisson, D. Gutman, L. Scarpace, S. N. Hwang, C. A. Holder, M. Wintermark, A. Rao, R. R. Colen, J. Kirby *et al.*, "Outcome prediction in patients with glioblastoma by using imaging, clinical, and genomic biomarkers: focus on the nonenhancing component of the tumor," *Radiology*, vol. 272, no. 2, pp. 484–493, 2014.

[17] J.-M. Lemée, A. Clavreul, and P. Menei, "Intratumoral heterogeneity in glioblastoma: don't forget the peritumoral brain zone," *Neuro-oncology*, vol. 17, no. 10, pp. 1322–1332, 2015.

[18] P. Prasanna, J. Patel, S. Partovi, A. Madabhushi, and P. Tiwari, "Radiomic features from the peritumoral brain parenchyma on treatment-naive multi-parametric mr imaging predict long versus short-term survival in glioblastoma multiforme: preliminary findings," *European radiology*, vol. 27, no. 10, pp. 4188–4197, 2017.

[19] J.-M. Lemée, A. Clavreul, M. Aubry, E. Com, M. De Tayrac, P.-A. Eliat, C. Henry, A. Rousseau, J. Mosser, and P. Menei, "Characterizing the peritumoral brain zone in glioblastoma: a multidisciplinary analysis," *Journal of neuro-oncology*, vol. 122, no. 1, pp. 53–61, 2015.

[20] J. Faget, S. Groeneveld, G. Boivin, M. Sankar, N. Zangger, M. Garcia, N. Guex, I. Zlobec, L. Steiner, A. Piersigilli *et al.*, "Neutrophils and snail orchestrate the establishment of a pro-tumor microenvironment in lung cancer," *Cell reports*, vol. 21, no. 11, pp. 3190–3204, 2017.

[21] N. Braman, P. Prasanna, J. Whitney, S. Singh, N. Beig, M. Etesami, D. D. Bates, K. Gallagher, B. N. Bloch, M. Vulchi *et al.*, "Association of peritumoral radiomics with tumor biology and pathologic response to preoperative targeted therapy for her2 (erbb2)–positive breast cancer," *JAMA network open*, vol. 2, no. 4, pp. e192 561–e192 561, 2019.

[22] M. Khorrami, M. Khunger, A. Zagouras, P. Patil, R. Thawani, K. Bera, P. Rajiah, P. Fu, V. Velcheti, and A. Madabhushi, "Combination of peri-and intratumoral radiomic features on baseline ct scans predicts response to chemotherapy in lung adenocarcinoma," *Radiology: Artificial Intelligence*, vol. 1, no. 2, p. 180012, 2019.

[23] X. Wang, X. Zhao, Q. Li, W. Xia, Z. Peng, R. Zhang, Q. Li, J. Jian, W. Wang, Y. Tang *et al.*, "Can peritumoral radiomics increase the efficiency of the prediction for lymph node metastasis in clinical stage t1 lung adenocarcinoma on ct?" *European radiology*, vol. 29, no. 11, pp. 6049–6058, 2019.

[24] N. Beig, M. Khorrami, M. Alilou, P. Prasanna, N. Braman, M. Orooji, S. Rakshit, K. Bera, P. Rajiah, J. Ginsberg *et al.*, "Perinodular and intranodular radiomic features on lung ct images distinguish adenocarcinomas from granulomas," *Radiology*, vol. 290, no. 3, pp. 783–792, 2018.

[25] C.-X. Wu, G.-S. Lin, Z.-X. Lin, J.-D. Zhang, L. Chen, S.-Y. Liu, W.-L. Tang, X.-X. Qiu, and C.-F. Zhou, "Peritumoral edema on magnetic resonance imaging predicts a poor clinical outcome in malignant glioma," *Oncology letters*, vol. 10, no. 5, pp. 2769–2776, 2015.

[26] S. Rathore, H. Akbari, J. Doshi, G. Shukla, M. Rozycki, M. Bilello, R. A. Lustig, and C. A. Davatzikos, "Radiomic signature of infiltration in peritumoral edema predicts subsequent recurrence in glioblastoma: implications for personalized radiotherapy planning," *Journal of Medical Imaging*, vol. 5, no. 2, p. 021219, 2018.

[27] T. Xiao, W. Hua, C. Li, and S. Wang, "Glioma grading prediction by exploring radiomics and deep learning features," in *Proceedings of the Third International Symposium on Image Computing and Digital Medicine*. ACM, 2019, pp. 208–213.

[28] S. Deepak and P. Ameer, "Brain tumor classification using deep cnn features via transfer learning," *Computers in biology and medicine*, vol. 111, p. 103345, 2019.

[29] Y. Yang, L.-F. Yan, X. Zhang, Y. Han, H.-Y. Nan, Y.-C. Hu, B. Hu, S.-L. Yan, J. Zhang, D.-L. Cheng *et al.*, "Glioma grading on conventional mr images: a deep learning study with transfer learning," *Frontiers in neuroscience*, vol. 12, 2018.

[30] M. Decuyper and R. V. Holen, "Fully automatic binary glioma grading based on pre-therapy mri using 3d convolutional neural networks," in *International Conference on Medical Imaging with Deep Learning*, London, United Kingdom, 08–10 Jul 2019. [Online]. Available: https://openreview.net/forum?id=H1eBD0pTY4

[31] J. Liu, Y. Sheng, W. Lan, R. Guo, Y. Wang, and J. Wang, "Improved asd classification using dynamic functional connectivity and multi-task feature selection," *Pattern Recognition Letters*, vol. 138, pp. 82 – 87, 2020.

[32] W. Zhao, J. Yang, B. Ni, D. Bi, Y. Sun, M. Xu, X. Zhu, C. Li, L. Jin, P. Gao *et al.*, "Toward automatic prediction of egfr mutation status in pulmonary adenocarcinoma with 3d deep learning," *Cancer medicine*, vol. 8, no. 7, pp. 3532–3543, 2019.

[33] L. Liu, J. Cheng, Q. Quan, F.-X. Wu, Y.-P. Wang, and J. Wang, "A survey on u-shaped networks in medical image segmentations," *Neurocomputing*, vol. 409, pp. 244–258, 2020.

[34] J. Liu, M. Li, W. Lan, F.-X. Wu, Y. Pan, and J. Wang, "Classification of alzheimer's disease using whole brain hierarchical network," *IEEE/ACM transactions on computational biology and bioinformatics*, vol. 15, no. 2, pp. 624–632, 2018.

[35] J. J. Van Griethuysen, A. Fedorov, C. Parmar, A. Hosny, N. Aucoin, V. Narayan, R. G. Beets-Tan, J.-C. Fillion-Robin, S. Pieper, and H. J. Aerts, "Computational radiomics system to decode the radiographic phenotype," *Cancer research*, vol. 77, no. 21, pp. e104–e107, 2017.

[36] B. H. Menze, A. Jakab, S. Bauer, J. Kalpathy-Cramer, K. Farahani, J. Kirby, Y. Burren, N. Porz, J. Slotboom, R. Wiest *et al.*, "The multimodal brain tumor image segmentation benchmark (brats)," *IEEE transactions on medical imaging*, vol. 34, no. 10, pp. 1993–2024, 2014.

[37] S. Bakas, H. Akbari, A. Sotiras, M. Bilello, M. Rozycki, J. S. Kirby, J. B. Freymann, K. Farahani, and C. Davatzikos, "Advancing the cancer genome atlas glioma mri collections with expert segmentation labels and radiomic features," *Scientific data*, vol. 4, p. 170117, 2017.

[38] S. Bakas, M. Reyes, A. Jakab, S. Bauer, M. Rempfler, A. Crimi, R. T. Shinohara, C. Berger, S. M. Ha, M. Rozycki *et al.*, "Identifying the best machine learning algorithms for brain tumor segmentation, progression assessment, and overall survival prediction in the brats challenge," *arXiv preprint arXiv:1811.02629*, 2018.

[39] S. Bakas, H. Akbari, A. Sotiras, M. Bilello, M. Rozycki, J. Kirby, J. Freymann, K. Farahani, and C. Davatzikos, "Segmentation labels and radiomic features for the pre-operative scans of the tcga-gbm collection," 2017.

[40] S. Bakas, H. Akbari, A. Sotiras, M. Bilello, M. Rozycki, J. Kirby, and Freymann, "Segmentation labels and radiomic features for the pre-operative scans of the tcga-lgg collection," 2017.

[41] C. Chen, X. Liu, M. Ding, J. Zheng, and J. Li, "3d dilated multi-fiber network for real-time brain tumor segmentation in mri," in *International Conference on Medical Image Computing and Computer-Assisted Intervention*. Springer, 2019, pp. 184–192.

[42] J. Fehr and H. Burkhardt, "3d rotation invariant local binary patterns," in *2008 19th International Conference on Pattern Recognition*. IEEE, 2008, pp. 1–4.

[43] L. Liu, P. Fieguth, Y. Guo, X. Wang, and M. Pietikäinen, "Local binary features for texture classification: Taxonomy and experimental study," *Pattern Recognition*, vol. 62, pp. 135–160, 2017.

[44] Y. Huang, C. Liang, L. He, J. Tian, C. Liang, X. Chen, Z. Ma, and Z. Liu, "Development and validation of a radiomics nomogram for preoperative prediction of lymph node metastasis in colorectal cancer." *Journal of clinical oncology: official journal of the American Society of Clinical Oncology*, vol. 34, no. 18, p. 2157, 2016.

[45] H. Peng, F. Long, and C. Ding, "Feature selection based on mutual information: criteria of max-dependency, max-relevance, and min-redundancy," *IEEE Transactions on Pattern Analysis & Machine Intelligence*, no. 8, pp. 1226–1238, 2005.

[46] N. V. Chawla, K. W. Bowyer, L. O. Hall, and W. P. Kegelmeyer, "Smote: synthetic minority over-sampling technique," *Journal of artificial intelligence research*, vol. 16, pp. 321–357, 2002.

[47] C.-Y. J. Peng, K. L. Lee, and G. M. Ingersoll, "An introduction to logistic regression analysis and reporting," *The journal of educational research*, vol. 96, no. 1, pp. 3–14, 2002.

[48] C. J. Burges, "A tutorial on support vector machines for pattern recognition," *Data mining and knowledge discovery*, vol. 2, no. 2, pp. 121–167, 1998.

[49] A. Liaw, M. Wiener *et al.*, "Classification and regression by randomforest," *R news*, vol. 2, no. 3, pp. 18–22, 2002.

[50] T. Chen and C. Guestrin, "Xgboost: A scalable tree boosting system," in *Proceedings of the 22nd acm sigkdd international conference on knowledge discovery and data mining*. ACM, 2016, pp. 785–794.

[51] J. Amin, M. Sharif, M. Raza, T. Saba, and M. A. Anjum, "Brain tumor detection using statistical and machine learning method," *Computer Methods and Programs in Biomedicine*, vol. 177, pp. 69–79, 2019.

[52] X. Bi, J. G. Liu, and Y. S. Cao, "Classification of low-grade and high-grade glioma using multiparametric radiomics model," in *2019 IEEE 3rd Information Technology, Networking, Electronic and Automation Control Conference (ITNEC)*. IEEE, 2019, pp. 574–577.

[53] G. Cui, J. Jeong, B. Press, Y. Lei, H.-K. Shu, T. Liu, W. Curran, H. Mao, and X. Yang, "Machine-learning-based classification of lower-grade gliomas and high-grade gliomas using radiomic features in multi-parametric mri," *arXiv preprint arXiv:1911.10145*, 2019.

[54] P. Lambin, E. Rios-Velazquez, R. Leijenaar, S. Carvalho, R. G. Van Stiphout, P. Granton, C. M. Zegers, R. Gillies, R. Boellard, A. Dekker *et al.*, "Radiomics: extracting more information from medical images using advanced feature analysis," *European journal of cancer*, vol. 48, no. 4, pp. 441–446, 2012.

[55] D. Shen, G. Wu, and H.-I. Suk, "Deep learning in medical image analysis," *Annual review of biomedical engineering*, vol. 19, pp. 221–248, 2017.

[56] D. Hu, H. Zhang, Z. Wu, F. Wang, L. Wang, J. K. Smith, W. Lin, G. Li, and D. Shen, "Disentangled-multimodal adversarial autoencoder: Application to infant age prediction with incomplete multimodal neuroimages," *IEEE Transactions on Medical Imaging*, pp. 1–1, 2020.

[57] S. Vajapeyam, D. Brown, P. Johnston, K. Ricci, M. Kieran, H. Lidov, and T. Poussaint, "Multiparametric analysis of permeability and adc histogram metrics for classification of pediatric brain tumors by tumor grade," *American Journal of Neuroradiology*, vol. 39, no. 3, pp. 552–557, 2018.

[58] K. Chang, H. X. Bai, H. Zhou, C. Su, W. L. Bi, E. Agbodza, V. K. Kavouridis, J. T. Senders, A. Boaro, A. Beers *et al.*, "Residual convolutional neural network for the determination of idh status in low-and high-grade gliomas from mr imaging," *Clinical Cancer Research*, vol. 24, no. 5, pp. 1073–1081, 2018.

[59] Z. Akkus, I. Ali, J. Sedlář, J. P. Agrawal, I. F. Parney, C. Giannini, and B. J. Erickson, "Predicting deletion of chromosomal arms 1p/19q in low-grade gliomas from mr images using machine intelligence," *Journal of digital imaging*, vol. 30, no. 4, pp. 469–476, 2017.

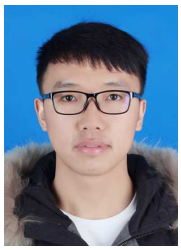

Jianhong Cheng received the B.S. degree from Liaoning Technical University, Fuxin, China, in 2014, the M.S. degree in software engineering from Central South University, Changsha, China, in 2017. And he is currently a Ph.D. candidate in School of Computer Science and Engineering, Central South University, Changsha, China. His research interests include machine learning, deep learning and medical image analysis.

Jin Liu received the PhD degree in computer science from Central South University, China, in 2017. He is currently a Lecturer at the School of Computer Science and Engineering, Central South University, Changsha, Hunan, P.R. China. His current research interests include medical image analysis, machine learning and bioinformatics.

Hailin Yue received the B.S. degree from NanJing XiaoZhuang University, Nanjing, China, in 2019. And he is currently a M.S. candidate in School of Computer Science and Engineering, Central South University, Changsha, China. His research interests include machine learning, deep learning and medical image analysis.

Harrison Bai received the B.S. degree in Yale University, USA, in 2008, the M.D. degree in Yale University School of Medicine, USA, in 2013, and the M.S. degree in Johns Hopkins University, USA, in 2017. He is currently an Assistant Professor of Diagnostic Imaging, Clinician Educator at University of Pennsylvania, USA. His current research interests include machine learning, medical image analysis, and related applications.

Yi Pan is a Regents' Professor of Computer Science and an Interim Associate Dean and Chair of Biology at Georgia State University, USA. Dr. Pan joined Georgia State University in 2000 and was promoted to full professor in 2004, named a Distinguished University Professor in 2013 and designated a Regents' Professor (the highest recognition given to a faculty member by the University System of Georgia) in 2015. He served as the Chair of Computer Science Department from 2005-2013. He is also a visiting Changjiang Chair Professor at Central South University, China. Dr. Pan received his B.Eng. and M.Eng. degrees in computer engineering from Tsinghua University, China, in 1982 and 1984, respectively, and his Ph.D. degree in computer science from the University of Pittsburgh, USA, in 1991. His profile has been featured as a distinguished alumnus in both Tsinghua Alumni Newsletter and University of Pittsburgh CS Alumni Newsletter. Dr. Pan's re-search interests include parallel and cloud computing, wireless networks, and bioinformatics. Dr. Pan has published more than 330 papers including over 180 SCI journal papers and 60 IEEE/ACM Transactions papers. In addition, he has edited/authored 40 books. His work has been cited more than 14000 times. Dr. Pan has served as an editor-in-chief or editorial board member for 15 journals including 7 IEEE Transactions. He is the recipient of many awards including IEEE Transactions Best Paper Award, 4 other international conference or journal Best Paper Awards, 4 IBM Faculty Awards, 2 JSPS Senior Invitation Fellowships, IEEE BIBE Outstanding Achievement Award, NSF Research Opportunity Award, and AFOSR Summer Faculty Research Fellowship. He has organized many international conferences and delivered keynote speeches at over 50 international conferences around the world.

Jianxin Wang received his B.S. and M.S. degree in Computer Science and Application from Central South University of Technology, P. R. China, and his PhD degree in Computer Science and Technology from Central South University. Currently, he is the dean and a professor in School of Computer Science and Engineering, Central South University, Changsha, Hunan, P.R. China. He is also a leader in Hunan Provincial Key Lab on Bioinformatics, Central South University, Changsha, Hunan, P.R. China. His current research interests include algorithm analysis and optimization, parameterized algorithm, bioinformatics and computer network. He has published more than 200 papers in various International journals and refereed conferences. He is a senior member of the IEEE. He has been on numerous program committees and NSFC review panels, and served as editors for several journals such as IEEE/ACM Trans. Computational Biology and Bioinformatics (TCBB), International Journal of Bioinformatics Research and Applications, Current Bioinformatics, Current Protein & Peptide Science, Protein & Peptide Letters.